Bio-Design and Manufacturing (2022) 5:189–200
https://doi.org/10.1007/s42242-021-00146-3

RESEARCH ARTICLE

Layout design and application of 4D-printing bio-inspired structures with programmable actuators

Siyuan Zeng[1] · Yixiong Feng[1] · Yicong Gao[1] · Hao Zheng[2] · Jianrong Tan[1]

Received: 7 January 2021 / Accepted: 9 June 2021 / Published online: 2 July 2021

Abstract

Four-dimensional (4D) printing is an advanced form of three-dimensional (3D) printing with controllable and programmable shape transformation over time. Actuators are used as a controlling factor with multi-stage shape recovery, with emerging opportunities to customize the mechanical properties of bio-inspired structures. The print pattern of shape memory polymer (SMP) fibers strongly affects the achievable resolution, and consequently influences several other physical and mechanical properties of fabricated actuators. However, the deformations of bio-inspired structures due to actuator layout are more complex because of the presence of the coupling of multi-directional strain. In this study, the initial structure was designed from closed-shell behavior and divided into a general unit and actuator unit, the latter responsible for driving the transformation. Mutual stress confrontation between the actuator and the general unit was considered in the layout thermodynamic model, in order to eliminate the transformation produced by the uncontrolled shape memory behavior of the general unit. Three critical and effective strategies for the layout design of actuators were proposed and then applied to achieve the desired accurate deformation of 3D-printed bilayer structures. Finally, the proposed approach was validated and adopted for fabricating a complex shell-like gripper structure.

Graphic abstract

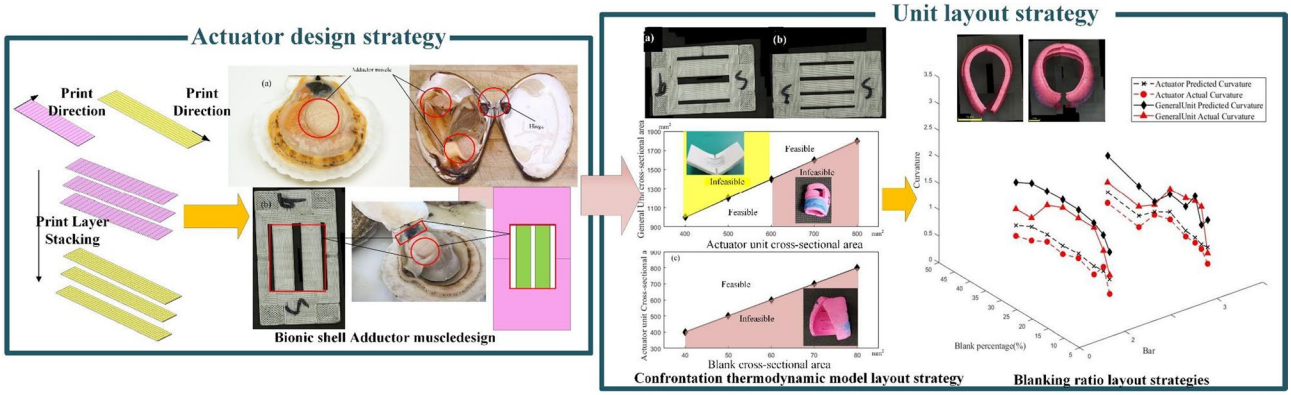

Keywords Bio-inspired structure · Layout design · Programmable actuators · Bilayer structure · 4D printing

✉ Yicong Gao
gaoyicong@zju.edu.cn

✉ Hao Zheng
haozheng@zju.edu.cn

[1] State Key Laboratory of Fluid Power and Mechatronic Systems, Zhejiang University, Hangzhou 310027, China

[2] Hangzhou Innovation Institute, Beihang University, Hangzhou 310000, China

Introduction

Traditional manufacturing techniques have become unsuitable for the fabrication of special structures in recent years; additive manufacturing (AM) is now widely used to fabricate increasingly complex three-dimensional (3D) structures [1–3]. Recently, a novel four-dimensional (4D) printing

method based on AM techniques and the use of smart materials such as memory polymers and memory alloys were reported [4, 5]. During 4D printing, a bio-inspired structure is deformed from two-dimensional (2D) to 3D by stimulating actuators [6, 7]. The 2D structure, which is the so-called initial structure, is fabricated by a 3D printer, and the desired 3D structure is formed upon stimulation [8]. The three fundamental stages of 4D printing are the preparation of the smart material configuration, the stimulation of the smart materials, and the programing of the printing process [9–11].

The transformation of the bio-inspired structure in 4D printing is driven by the actuators, which are made from smart materials [12–14]. These materials are stimulated in various ways such as the variation of temperature, the concentration of a specific ion, or magnetic control [15]. Fixtures and underwater vehicles designed to mimic biological movements have become hotspots for research on smart materials [16, 17]. Among such materials, shape memory polymers (SMPs) used to make temperature-driven actuators have a wide range of bio-inspired applications [18]. Temperature-driven 4D printing is mainly achieved by stimulation near the SMP glass transition temperature (T_g) [19]. The application of SMPs in 4D printing is based on the combined effect of thermal mismatches and glass transitions [20]. When an SMP exhibits a glass state below T_g, the strain caused by the mismatch of internal stress is insufficient to transform structures. When the temperature exceeds T_g, however, the modulus of the SMP is increased, resulting in a transition from glass to rubber state, which is related to a change in the thermal expansion coefficient [21]. In the process of fused deposition modeling (FDM), the first squeeze of the printing wire is carried out under heat. Once the structure has cooled down, the adhesion between the printing wires and the stretching of the printing wire itself is stored in the structure [18, 22]. These residual stresses are released during the second stimulation. In addition to direct heating, Joule heating and light heating are applied to temperature-driven actuators, which are more flexible than other forms of transformation [23, 24].

The initial structure design was later adjusted to realize bio-inspired structure folding and cutting technologies using SMPs [10, 25]. The fabrication of complex bio-inspired structures requires the simultaneous configuration of SMPs, the stimulation of smart materials, and the programming of the printing process [26, 27]. In previous studies, many deformation modes for the actuator were proposed, and thermodynamic models with high accuracy were developed [28]. In particular, forming mechanisms have been presented for actuators in the form of bilayer structures fabricated by direct formation or FDM [12]. However, when the mechanism is applied to the design of complex structures, the transformation accuracy decreases [11, 29]. This is due to the fact that no unit outside the actuator is usually considered involved in the deformation. Nonetheless, units other than the actuator are in fact also deformed during the 4D printing process using SMPs, due to the shape memory effect widely present in the polymer [30, 31]. Therefore, the printing pre-program and layout pre-division for the fabrication of a complicated structure are very important [32, 33].

The present study developed a layout design method for a bio-inspired structure. A bio-inspired structure is divided into a general unit and an actuator unit in FDM 4D printing [34]. By considering the thermodynamic interface between the two units, the accuracy of 4D printing transformation is improved and the molding of the wrapping and vertical transformation reduces the defects [35, 36]. Firstly, three critical and effective strategies for the layout design of actuators are proposed and then applied to achieve the desired accuracy of deformation of bio-inspired structures. The rest of this paper is organized as follows: In "Materials and methods" section, we describe the use of an FDM 3D printer and polylactic acid (PLA) to select the basic printing parameters for 4D printing, and the transformation modes of the actuator and general unit are analyzed. "Results and discussion" section entails basic strategies for actuator deformation and unit layout. Experiments are also performed to investigate the effect of the selected actuator aspect ratio transformation on actuator strain prediction. A detailed actuator layout strategy is then devised to ensure that the unit completed the deformation. Further verification of the proposed method is included in the example of a gripper design. "Conclusions" section concludes the paper with a discussion on potential further research.

Materials and methods

Materials

A method of 4D printing with homogeneous material using internal stress was used to reduce the manufacturing difficulty and limit the number of external variables [11]. This method of 4D printing can take advantage of SMP shape memory behavior without applying initial external forces [31, 37]. The SMP PLA used in this paper was purchased from Ultimaker ('Tough PLA') and stored under vacuum to prevent degradation and reduce the effects of atmospheric humidity. The normal allowable linear thermal expansion coefficient and elastic modulus of the material were measured by differential scanning calorimetry (DSC) and dynamic thermomechanical analysis (DMA) tests, respectively. Glass transition temperature T_g is 65 °C, the modulus at room temperature is 3523 MPa, and melting temperature T_m is 183 °C.

Bio-inspired structure with programmable actuators

The deformation of bio-inspired 4D structures is mainly achieved via the actuators. Shell organisms in nature achieve the closure of both shell sides by means of the shell-closing muscles, as shown in Fig. 1 [38]. Figure 1a illustrates the adductor muscle and hinge of the shell organism, where the deformation of the hinge is controlled by the contraction of the adductor muscle. The designed bio-inspired structure is shown in Fig. 1b. Through the combination of adductor muscle and hinge, the actuator has the function of both organs. The 4D printing deformation process requires the use of actuators, as shown in the red box of Fig. 1b, which deform the structure into its programmed shape when stimulated.

The pink area on the right side of Fig. 1b is the general unit of bio-inspired structure, which resembles the shell of a shell organism. When the adductor muscle performs a closing action, the shell exerts some inhibition on the action of the adductor muscle. Although the deformation of the general unit is usually smaller than that of the actuator unit, it is multi-directional. The shell gripper is used as an example in this paper. It is noteworthy that general units other than the actuator also participate in the deformation process, which inhibits the deformation of the actuator and makes the process inaccurate.

The general unit reduces the deformation error of the actuator by preventing interconnections, as shown in Fig. 1. In order to better validate the theory, this study adopts the general connected design method. The actuator uses a bilayer structure, which allows for precise control when adopting the 4D printing method described above through varying the process conditions while retaining a large value of strain [39].

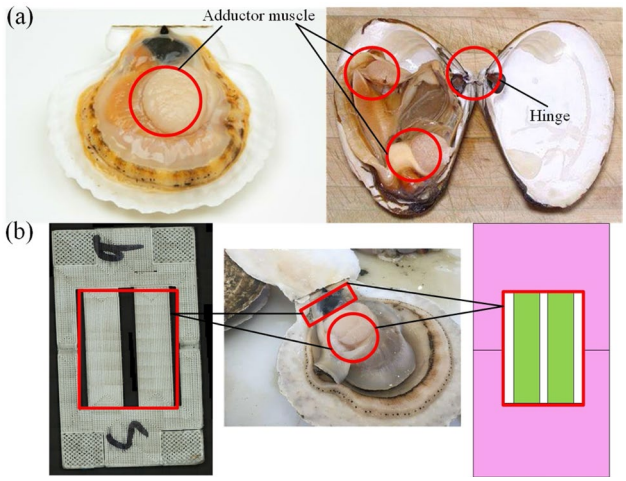

Fig. 1 Bio-inspired structure with actuators: (**a**) adductor muscle and hinge of shell; (**b**) bio-inspired structure with programmable actuator

Assessment of impacts on actuator

In order to limit unknown variables in the experiment and determine the material parameters, Ultimaker PLA was used as the material for FDM printing. A heterogeneous print unit effect was created by changing the PLA printing process. This allows the 4D printing process to be implemented in a simple primary print and secondary stimulation, while avoiding the unclear mechanism of bonding between unit joints [28, 40]. A digital optical microscope was used to observe sectional images of the printed units. A high-precision water bath was utilized for uniform heat transformation within the initial structure.

In 4D printing, the thermal expansion coefficient of each material layer is controlled by changing the process parameters [41]. The process flow of FDM 4D printing based on process parameters is as follows: Firstly, the thermo-mechanical mechanism of the bilayer structure actuator is analyzed, and the deformation behaviors of the SMP are modeled. A computer aided design (CAD) model of the structure is then sliced into 2D images for 3D printing. In the meantime, SMP materials are fabricated into 3D printing consumables. Next, the surrogate model with main deformation programming parameters, including line width, print height, print temperature, filled form, and stimulation temperature, are fitted by the orthogonal experiment and response surface method. The permanent deformation of the bilayer structure actuator results from the programmed parameters and time evolution of the 3D printed structure upon heating. The most relevant parameters of the linear thermal expansion coefficient are printing temperature, printing line height, printing line width and printed filling pattern. The basic transformation principle for a bilayer actuator arises from the anisotropy of stress between the two layers, which is provided by thermal expansion or memory behavior [40]. The linear thermal expansion coefficient under unit temperature change can be expressed as strain. Different PLA material strains derived from single variable experiments are shown in Fig. 2. Figure 2a demonstrates that the linear thermal expansion coefficient decreases with printing temperature rising within a certain range in which the SMP is viscous: 192–242 °C. As shown in Fig. 2b, in the 40–220 μm print height range, the higher the print line height, the lower the linear thermal expansion coefficient. As observed in Fig. 2c, when the print width is in the range of 0.15–0.80 mm, the greater the print line width, the higher the linear thermal expansion coefficient.

The control of 3D printing parameters in 4D printing deformation appears to be a composite process; the effect of a single parameter on deformation is one-sided. In addition, it is the printed pattern that controls the direction of strain in the 3D coordinate plane during the second stimulation. The strain is essentially the same in both directions, except for the partial pattern. In order to achieve the maximum strain in

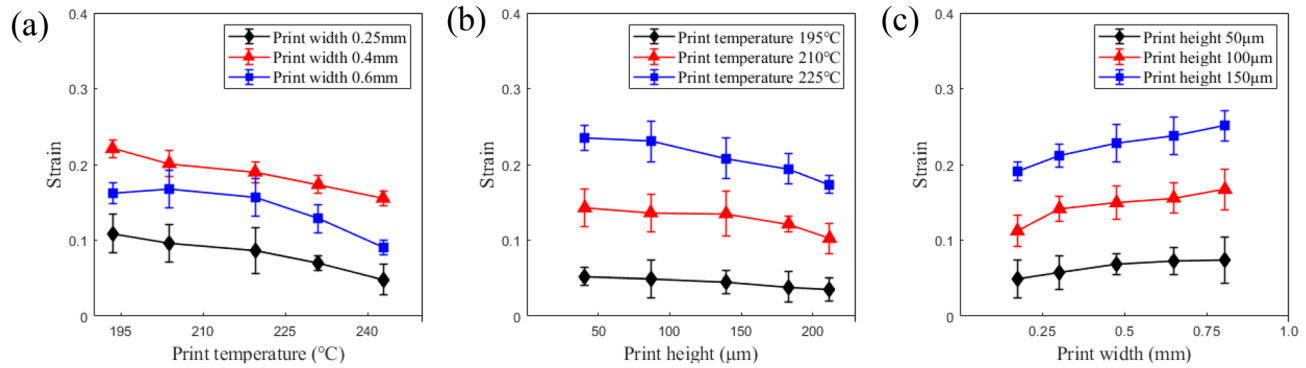

Fig. 2 Effects of process parameters on strain: (**a**) the strain change of PLA with the print height set as 0.20 μm; (**b**) the strain change of PLA with the print width set as 0.20 mm; (**c**) the strain change of PLA with the print temperature set as 195 °C

the bilayer structure, in this paper, the upper and lower filling patterns in the bilayer actuator were horizontal and vertical stripes, respectively. The horizontal and vertical stripes in the actuator consisted the same printing parameter, and the printing direction was vertical, with a horizontal direction strain of 3.5 and longitudinal strain of 1.1. The grid patterns used for the general unit were similar (the transverse and longitudinal strain was 0.125).

Actuator layout that considers 'coupling'

Due to the actuator strain being multi-directional, it is difficult to arrange all the actuators on the center of the initial structure to avail the transformation of complex structures. The areas of the general unit and the actuator unit must match each other. In Fig. 3, the yellow and pink areas are the actuator unit and the general unit of an initial foldable structure, respectively. Within the general units, there are also parts such as the red dotted line, which are not directly acted upon by the actuators, but function more independently. The strain is predominant but is driven by the strain of the blue dashed line. The deformations of the bilayer actuator possess anisotropic characteristics, and need to be matched to the general unit. However, the models are different in each connected region, thus it proves difficult to lay out the units in the initial structure.

In order to verify the accuracy of the model, this study used the conventional unit-connected design method, which must take into account the stresses on the red axis. A certain gap is reserved in the actuator unit to allow the actuator to complete the deformation.

Fabrication of bio-inspired structures

The fabrication of the initial structure was achieved by pre-editing before 4D printing. An initial 3D model of the complex structure was first designed, and the deformation shape of the bilayer actuator was preset by programming the printing process. Next, the configuration of printing units was set out, and a reasonable printing pattern was selected to determine the deformation direction of the stress–strain. Finally, the matching printing temperature and stimulation temperature were determined by the thermodynamic cycle relationship, and printing was completed in the 3D printer. The details are shown in Fig. 4, and the instruments used in the experiment are listed in Table 1.

The process parameters were: 195 °C printing temperature, 50 μm printing line height, 90 °C stimulation temperature, and 0.4 mm printing line width. In the 80 mm × 40 mm

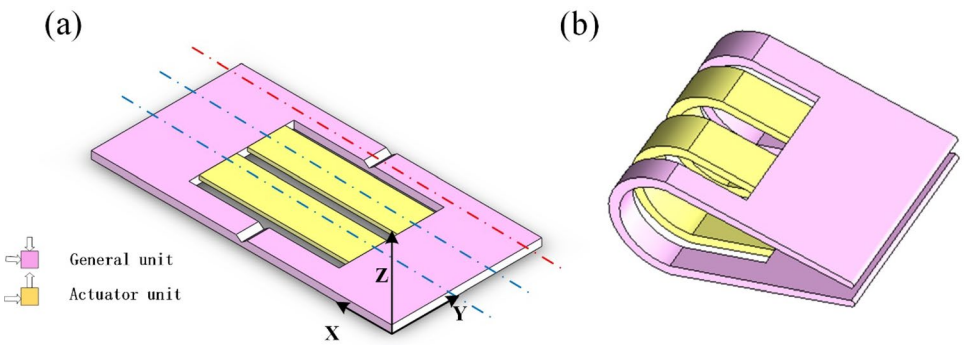

Fig. 3 Initial structure with general unit and actuator unit (**a**) and deformed structure with general unit and actuator unit (**b**)

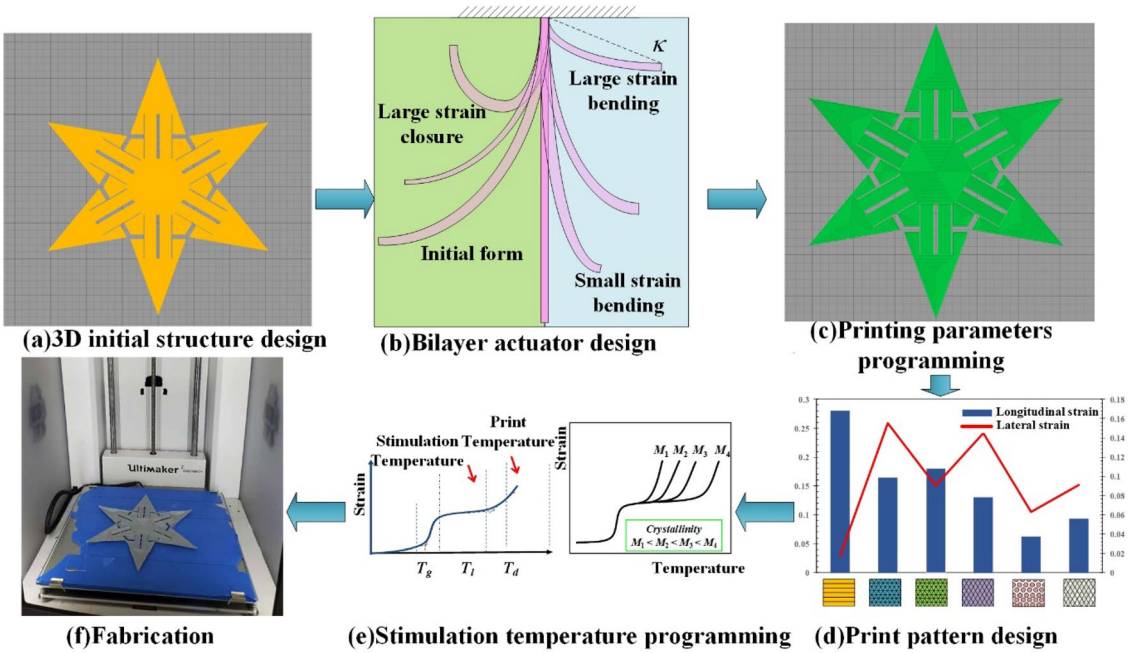

Fig. 4 Illustration of proposed approach for fabricating 3D complex structures: (**a**) 3D initial structure design; (**b**) bilayer actuator design; (**c**) printing parameters programming; (**d**) print pattern design; (**e**) stimulation temperature programming; (**f**) fabrication

Table 1 Experimental equipment

Name	Elastomer
3D Printer	Ultimaker2 Extend +
Microscope	Olympus DSX110 3.5 × objective lens
Water bath	Lichen HH-8

printing plane, the usable area was about 1060–2120 mm^2. The total shape size of the initial foldable structure was set as 80 mm × 40 mm × 2 mm. In addition, the actuator unit and general unit were printed in each print layer using 3D editing software. The upper and lower actuators had a height ratio of 1/1 and 1/3 layout in the actuator unit, as required.

Deformation structure characterization

Stimulation for the printed initial structure was performed in a 90 °C water bath heater unit. The product was allowed to cool down and was removed after complete deformation to reduce any error caused by the operation. The deformation was measured by the Olympus DSX system mainly in terms of curvature. As shown in Fig. 5, the deformation structure was measured in two main forms: the curvature lines of the two units intersected in one, and they did not intersect in the other. The average curvature of the deformed unit was obtained from five isometric measurements; the yellow and green dashed lines in the figure are schematic diagrams of separate single measurements.

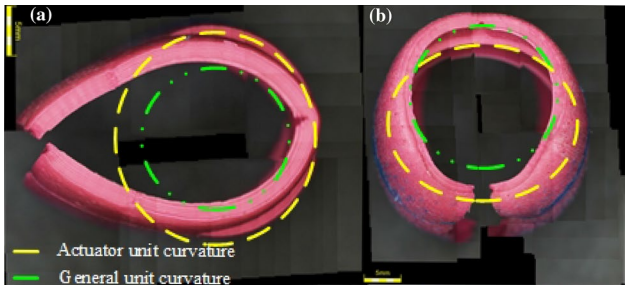

Fig. 5 **a** Curvature measurement of the non-intersecting curvature lines of the general unit and the actuator unit. **b** Curvature measurement of the intersecting curvature lines of the general unit and the actuator unit

Results and discussion

Influence of actuator design parameters

Design strategy 1 Actuator deformation was made to produce the desired deformation by pre-programming the actuator printing parameters.

In the initial structure folding, the actuator unit needs to vertically and horizontally move upward. According to analysis with Timchenko beam, the bilayer structure

expands in the vertical direction in the 2D plane and shrinks in the horizontal direction [42], while the general unit shrinks in both directions. The upper and lower edges of the bilayer actuator are connected to the general unit, and the radial force of the general unit is applied to both ends of the bilayer actuator. As shown in the literature [39], according to the equilibrium relationship, the linear thermal expansion coefficient can be expressed in terms of curvature. The bilayer actuator has an anisotropic relationship on the connection x-axis in the direction shown by the dashed blue line in Fig. 3a, as follows:

$$\begin{cases} \kappa_a = \dfrac{(\alpha_2-\alpha_1)(t-t_0)}{\frac{h_{\text{total}}}{2}+\frac{2(E_1I_1+E_2I_2)}{h_{\text{total}}}\left(\frac{1}{E_1a_1}+\frac{1}{E_2a_2}\right)}, \\ \varepsilon_r = (\alpha_2-\alpha_1)(t-t_0), \end{cases} \tag{1}$$

where α_2 and α_1 are the thermal expansion coefficient of the two layers, h_{total} represents the total thickness of the structure, E_1 and E_2 are the elastic modulus of the two layers, I_1 and I_2 represent the bending coefficient of the two layers, and a_1, a_2 are the thickness of each layer of bilayer actuator.

For a given design space, the transformation of all units needs to be programed. The linear thermal expansion coefficient can be expressed in terms of curvature. In order to fully fold the initial structure, the total area of the actuator unit was set to 40 mm × 20 mm to 40 mm × 30 mm. The thickness ratio was set to 1:1 to better control the transformation. The x-axis length was fixed at 40 mm, and the effect of the aspect ratio was verified by changing the y-axis length. As shown in Fig. 6a, when the actuator was positioned, increasing the length of the x-axis changed the direction of the strain on the z-axis due to the induction of y-axis strain.

For a single actuator, the longitudinal axis can be analyzed based on Eq. (1). In the 4D printed bilayer actuator, however, the applied stress is not only in one direction. In the horizontal and vertical configuration of the bilayer structure, both the transverse and longitudinal tensile stresses of the bilayer structure actuator form a stress gradient difference after stimulation, as shown in Fig. 3a. Thus, the underlying yellow layer expands in the x-axis direction and contracts in the y-axis direction for the

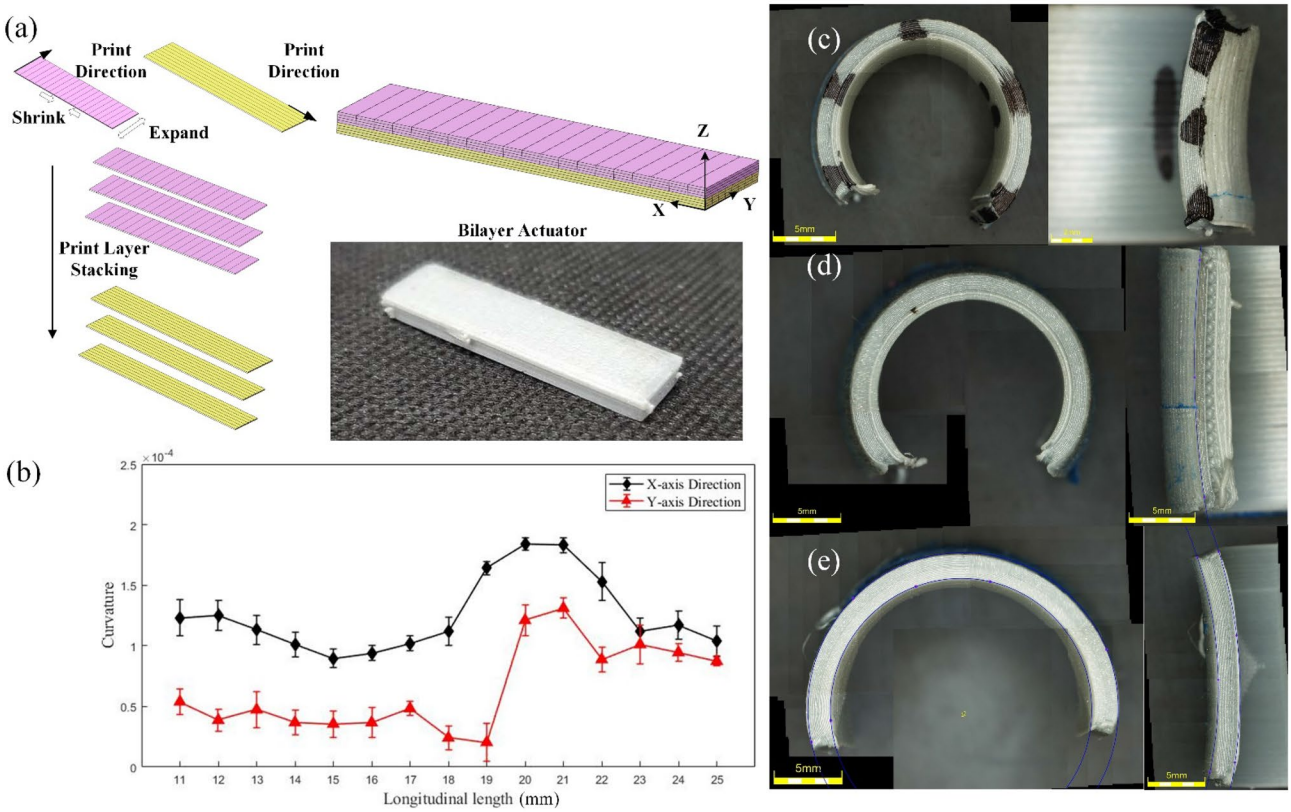

Fig. 6 **a** 3D printing x- and y-axis strain for bilayer actuator. **b** Curvature of x- and y-axis transformation of actuators of different lengths. **c** 40 mm x-axis length, 11 mm y-axis length transformation on both sections of the actuator. **d** 40 mm x-axis length, 20 mm y-axis length transformation on both sections of the actuator. **e** 40 mm x-axis length, 25 mm y-axis length deformation on both sections of the actuator

selected FDM print pattern. The top pink layer expands in the *y*-axis and contracts in the *x*-axis. The linear thermal expansion coefficients of the horizontal and vertical lines for the same printing strategy are the same in each vertical direction. In the horizontal and vertical configuration of the bilayer actuator, the lateral and longitudinal tensile stresses of the bilayer structure actuator are stimulated to form a stress gradient difference. The mismatch of lateral and longitudinal stresses results in combined strain along the *z*-axis in the positive direction. However, viewing the structure in the *x*-axis direction produces strain in the negative *z*-axis direction, since the two layers are printed from the same pattern perpendicular to each other.

In Fig. 6b, the curvature of the structure at two different cross sections is given for a constant *x*-axis direction length of 40 mm and a *y*-axis direction length of 11–25 mm. For the first type (Fig. 6c), the actuator had a 40 mm *x*-axis length and 11 mm *y*-axis length. The strain in the *x*-axis decreased due to a combination of *x*- and *y*-axis stresses, while the ratio exceeded 1:2. Due to the curvature induced by the *x*-axis, the direction of the integrated stress was represented by the positive *z*-axis, and increasing the length of the *y*-axis would offset this curvature. For the second type (Fig. 6d), the actuator had 40 mm *x*-axis length and 20 mm *y*-axis length. When the structure reached 20 mm in size, due to the stress action in the *y*-axis direction being reduced to a similar phase, the transverse and longitudinal curvature of the structure increased, the strain became close to the maximum, and the curvature peaked at around 20 mm. For the second type (Fig. 6e), the actuator had 40 mm *x*-axis length and 25 mm *y*-axis length. When the length-to-width ratio exceeded 1.82, the structure tended to twist and the transformation could be not easily controlled.

In order to precisely control the transformation, even if there is a peak at about 1/2, the actuator should be selected with an aspect ratio as low as 1/2. The influence of actuator on the overall initial structure was adjusted by varying the number of lateral layouts within the internal structure. In this study, actuators with a width of 20 mm or less of two types were selected: two-bar layout and three-bar layout.

Layout design and fabrication of bio-inspired structure

Design strategy 2 The layouts of the actuator and general unit are designed by means of the thermodynamic model, while considering the coupling interaction between the two units.

On the basis of Eq. (1), the layout between units and the layout of the actuator in the actuator unit are considered and combined with the general unit.

Let

$$\frac{\alpha_1}{\alpha_2}=m,\ \frac{\alpha_1}{\alpha_3}=k,\ \frac{\alpha_2}{\alpha_3}=l,\ \frac{E_1}{E_2}=n,\ \frac{E_1}{E_3}=g,\ \frac{E_2}{E_3}=j,$$

where α_3 and E_3 are the linear thermal expansion coefficient/elastic modulus and bending coefficient of the general unit, respectively.

The contraction of the general unit is not considered in Eq. (1), and the general unit contracts in both layers, producing facilitation and inhibition, respectively. Subsequently, Eq. (1) becomes

$$\begin{cases} \kappa_a = \dfrac{24\Delta\varepsilon_g\left(t-t_0\right)}{h_{\text{total}}\left[3\left(1+m^2\right)+\alpha_3^2\left(\frac{1}{gk}+\frac{1}{jl}\right)\left(14+n+\frac{1}{n}\right)\right]}, \\ \Delta\varepsilon_g = \left(\alpha_3-\dfrac{\alpha_1+\alpha_2}{2}\right)\left(t-t_0\right). \end{cases} \tag{2}$$

According to Eq. (2), the strain of the general unit affects the strain of the actuator unit, and it is difficult to control the strain of the general unit with precise stimulation in the temperature-driven strategy. In order to make the strain of the actuator unit approach the expected value, a_3 and e_3 need to be as low as possible. As a result, the strain of the general unit will be lower. As shown in Fig. 7 the curvature increases with $\Delta\varepsilon_g$. Through the decrease in $\Delta\varepsilon_g$, the cover problem of the initial structure is reduced. However, there is significant deviation from the distance expectation [43]. As shown in Fig. 3a, the general unit curvatures in the blue axial direction are expressed as

$$\kappa_{gb}=\frac{\left(\alpha_2-\alpha_1\right)\left(t-t_0\right)}{\frac{h_{\text{total}}}{2}+\frac{2\left(E_1I_1+E_2I_2\right)E_3I_3\alpha_3\left(t-t_0\right)}{h_{\text{total}}}\left(\frac{1}{E_1\alpha_1}+\frac{1}{E_2\alpha_2}\right)\left(\frac{1}{E_1\alpha_1}-\frac{1}{E_2\alpha_2}\right)}. \tag{3}$$

Thus, the general unit curvature in the red axis can be expressed as

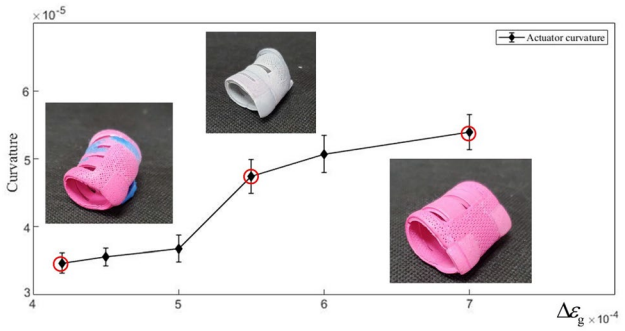

Fig. 7 Effect of strain on initial transformation

$$\kappa_{gr} = \frac{6(\alpha_2 - \alpha_1)(t - t_0)(1+m)^2}{h_{\text{total}}\left[3(1+m^2) + a_3^2 \Delta\varepsilon_g (1+mn)\left(\frac{1}{gk} - \frac{1}{jl}\right)\left(m^2 + \frac{1}{mn}\right)\right]}. \tag{4}$$

Design strategy 3 Design the layout blanking ratio in the actuator unit and adjust the size of the actuator so that the initial structure deforms as expected.

In an actual transformation process, the blank of actuators in the cross section of the actuator unit also determines whether it can complete the expected function. Even if the actuators do not touch each other in the initial structure, they may touch during the transformation due to radial stress. This is due to the fact that the vertical stress is not considered during the layout process. However, considering the strain caused by these stresses in a thermodynamic formula would make the design process highly complicated, and the final results too difficult to obtain. The contact of these structures during the heating process can be avoided to a certain extent. Therefore, a clearance in the unit arrangement is required to allow for close to expected transformation. The layouts with two-bar actuators and three-bar actuators are shown in Fig. 8a and 8b, respectively. The lower part of Fig. 8 shows the feasible deformation relationship between the area of the two units and actuator blank area for the two-bar and three-bar actuators.

Figure 8c presents the relationship between the blank in the actuator and the actuator unit cross-sectional area in the form of a blank percentage. When the ratio of the actuator and blank is too low, the initial structural transformation will be infeasible and cannot follow the z-axis, as shown in the sample of red area in Fig. 8c. The relationship between the actuator unit and general unit cross-sectional areas is presented in Fig. 8d. With a low actuator unit volume, the actuator strain is insufficient to drive the general unit. As a result, the structure is infeasible as shown in the sample of yellow area in Fig. 8d. When the actuator unit is oversized, the actuator is infeasible due to the actuators pressing against each other, as shown in the sample of red area in Fig. 8d. Figure 8e demonstrates the relationship between the general unit and blank cross-sectional areas when the actuator unit is fixed. If the general unit is too small, the collision between the actuators and the collision between the actuator unit and general unit make the transformation infeasible, as shown in the sample of yellow area in Fig. 8e. Due to the incomplete transformation of the collapsible structure, the structure will be infeasible if the general unit is too large, as shown in the sample of red area in Fig. 8e. Considering the molding limits in the configuration of two-bar and three-bar actuators, reserved spaces of 8–40% and 10–40%, respectively, are chosen.

The experimental variables are mainly controlled by placing the blank between the actuator unit and the general

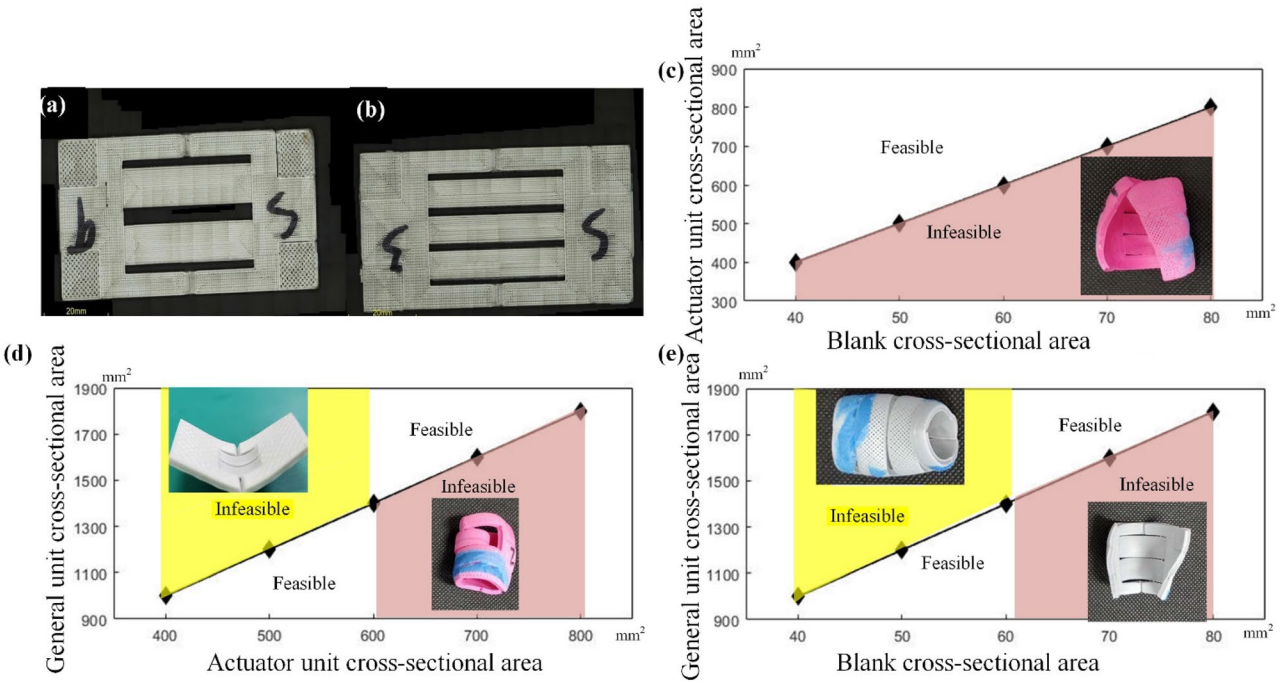

Fig. 8 Two-bar (**a**) and three-bar (**b**) actuator initial structures. **c** Actuator unit and blank cross-sectional areas. **d** General unit and actuator unit cross-sectional areas. **e** General unit and blank cross-sectional areas

unit. The strain in the *x*-axis direction (folding direction) is programmed as described in "Influence of actuator design parameters" section. However, the *y*-axis perpendicular to the folding direction is highly unfavorable for planning. Therefore, when the actuator to be used is acting alone, there should be a blank on both sides in the *y*-axis direction. Resulting transformations in the *x*-axis direction are basically deformations under a small, complete-suppression condition.

Since material conservation and strain in the *x*- and *y*-axis cause the vertical strain to decline, there is error in the *y*-axis direction. However, the trend of *x*- and *y*-axis strain does not change. If the blank actuator unit has a total reserved space of 10–40% with order (printing with a uniform distribution), the expected transformation can be solved by Eq. (4). The actual and predicted actuator curvature and the actual and predicted general unit curvature are given for a blank percentage at 10–40%, respectively, in Fig. 9. For a stimulation unit consisting of two-bar actuators, when the actuators do not directly contact one another on the *y*-axis, the strain in the *x*-axis direction reaches 8%. Therefore, the actuator needs to be set to a blank percentage of 10% or more to achieve the set curvature. Moreover, the blank of the layout cannot exceed 30% under such planning. Performing the

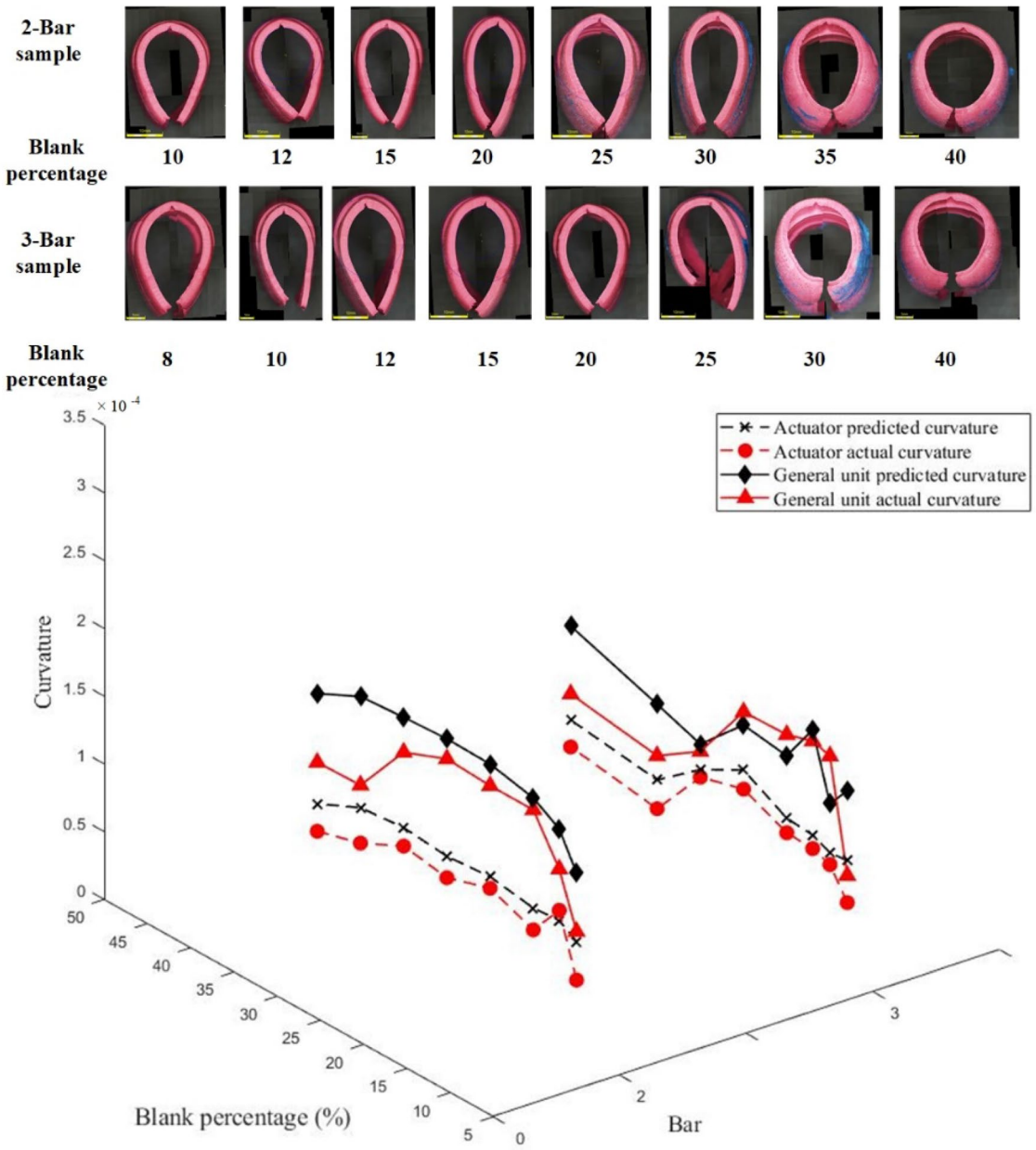

Fig. 9 Transformation curvature experiments with different bars and blank percentages

same analysis steps for the reserve space for single- and triple-actuator layouts indicates that the reserve space required for three actuators is an approximately 12% increase in the *z*-axis transformation rate, and one actuator is difficult to adapt to the transformation space to achieve transformation. Therefore, predictions for the actuator unit and general unit are more accurate in the 12–30% range.

In the uniaxial process, due to the conservation of material mass, the error is within a certain margin. Within a particular blank range for a two-bar suppressor or three-bar suppressor actuator, accurate strain prediction of the initial structure can be made. When the blank range is too small, the internal stress in the *y*-axis direction will be too large to achieve the expected transformation of the structure. When the blank range is too large, the actuator itself will be inherently less deformed and more suppressed by general units, making predictions inaccurate. However, the total curvature precision of the two structures is similar for the same expected transformation in the exact range.

The one-sided analysis process with Timoshenko beam simplifies the design process through calculations, and the transformation trends and forces become correct and accurate. However, due to its uniaxial nature, stresses in both the *x*- and *y*-axis directions of the general unit are transmitted to the actuator, which is the main cause of errors in prediction within a controlled range. The *y*-axis stress of the general unit also affects the structure. This is another major cause of inaccurate predictions, i.e., when the gaps are too large and this is one of the causes of error in the accuracy interval. Moreover, the conservation of mass of the material itself is not considered in complex structures, resulting in large errors.

Application example

In order to fully verify the clamping weight performance, as well as the clamping flexibility of the shell fixture, two fixtures were designed for clamping three different objects. The proposed design and fabrication method was employed to build two kinds of shell gripper for Structure1 (size: 150 mm × 80 mm × 3.5 mm) and Structure2 (size: 80 mm × 40 mm × 2 mm), which grasped an egg / irregularly surfaced model, and grasped a T-piece, respectively. Shell grippers were lowered and raised at a uniform speed of 5 mm/s using tin wire traction, the grabbing process was timed from 2 s after submerging into the water, and the object was fully dragged 2 s after the end of the timing. The weights of Structure1 and Structure2 were 38 g and 17 g, respectively. In the three experiments, the egg in the first experiment weighed 43 g, the handle in the second experiment weighed 52 g, and the T-shaped workpiece in the third experiment weighed 18 g.

The grasping process for the two different structure sizes is given in Fig. 10. Structure1 grasped the egg and irregularly surfaced model, and Structure2 grasped the T-piece, respectively. Since the sizes of grasped objects were greater than the expected external curvature, all grasps were successful. As shown in Fig. 10a, Structure1 required 40 s to complete the egg grasping; as shown in Fig. 10b, Structure1 required 32 s to complete the irregularly surfaced model grasping. Meanwhile, the T-piece gripping using Structure2 required 15 s, as shown in Fig. 10c. Both gripping results for Structure1 were satisfactory, and it is concluded that the same configuration of the shell gripper can be adapted to different gripping requirements. The proposed gripper is flexible to ensure that the object is not damaged when the outer curvature is smaller than the size of the gripped object. This strategy achieves heterogeneous unit performance by programming the *z*-axis strain of each unit, as well as the layout of the units within each print plane, with particularly good results for different print planning processes for the same material.

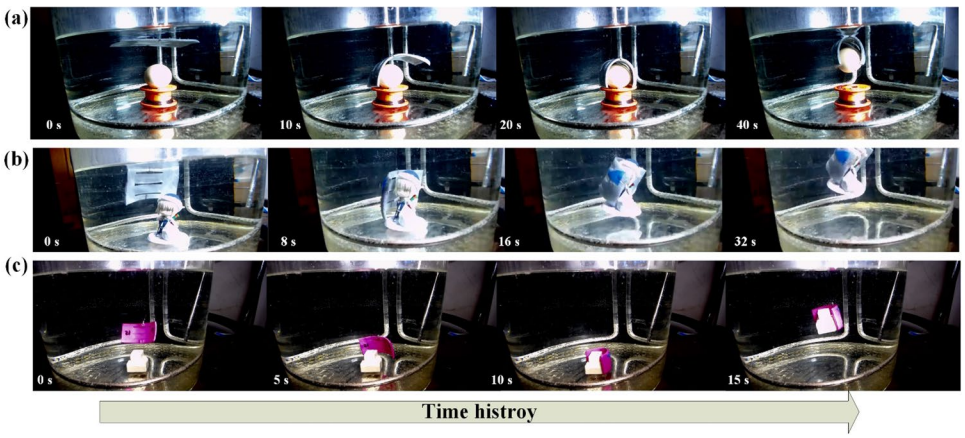

Fig. 10 Actions of shell gripper of egg over time (**a**), shell gripper of irregularly surfaced model over time (**b**) and shell gripper of T-shaped structure over time (**c**)

Conclusions

In this study, efficient bio-inspired 4D printing layout strategies were developed by designing the area delineation and shape memory properties of SMP materials, and a bio-inspired structure was fabricated by imitating a shell in order to test the proposed layout design. Four-dimensional printing using FDM was realized by dividing the initial structure of 4D printing into a stimulation unit and general unit with the SMP material PLA. Using a desktop-level 3D printer, the process parameters were programmed so that different heterogeneous units were made from the same material. The exposure of the units to the same stimulus subjected them to different strains. The stress–strain equations for each unit were derived by analyzing their individual thermodynamic behaviors. The actuator unit takes advantage of the anisotropy of the bilayer structure, to enable the structure to collapse by the strain on the axis occurring from the stresses on the x- and y-axis.

The relationship between the strain direction of the actuator within the actuator unit and the size of the structure was verified, and the initial structural strain was brought further near to that expected by reserving free space in the stimulation unit. The adoption of the new model under the steady-state model brought the transformation of the initial structure closer to the expectations. At the same time, the permissible range for the model was analyzed and the probability of various molding defects was reduced by regulating the voids inside the actuator unit. Two kinds of shell gripper were designed using this strategy, which can successfully grip eggs with complex T-shaped structures and fragile shells. These grippers are useful for flexible grasping in complex environments. The proposed strategies consider less general unit transformation in other 4D units, which greatly improves manufacturing accuracy and simplifies the design process, especially in 4D printing via FDM. To improve the usefulness of 4D printing, future work could reconstruct the proposed thermodynamic model and use the strategy to create robotic grippers or hydrodynamic surfaces in more complex structures. The strategy could also be used with primary stimulation in the form of geomatics or light-cured 4D printing.

Acknowledgements This work was supported by the National Natural Science Foundation of China (Nos. 51805472, 51775489, and 51975386), and the Natural Science Foundation of Zhejiang Province, China (No. LZ21E050004).

Author contributions SYZ and YCG proposed the method. SYZ conducted experiments, processed the experimental data and wrote the manuscript. YCG helped to design experiments and revised the manuscript. HZ provided some ideas about the experiments and helped to edit the paper. JRT and YXF gave some advices about the proposed method. All authors did a favor for the final manuscript.

Data availability The raw/processed data required to reproduce these findings cannot be shared at this time as the data also form part of an ongoing study.

Declarations

Conflict of interest The authors declare that there is no conflict of interest.

Ethical approval This article does not contain any studies with human or animal subjects performed by any of the authors.

References

1. Khoo ZX, Teoh JEM, Liu Y et al (2015) 3D printing of smart materials: a review on recent progresses in 4D printing. Virtual Phys Prototy 10(3):103–122. https://doi.org/10.1080/17452759.2015.1097054
2. Momeni F, Hassani SMMN, Liu X et al (2017) A review of 4D printing. Mater Des 122:42–79. https://doi.org/10.1016/j.matdes.2017.02.068
3. Rastogi P, Kandasubramanian B (2019) Breakthrough in the printing tactics for stimuli-responsive materials: 4D printing. Chem Eng J 366:264–304. https://doi.org/10.1016/j.cej.2019.02.085
4. Choong YYC, Maleksaeedi S, Eng H et al (2017) 4D printing of high performance shape memory polymer using stereolithography. Mater Des 126:219–225. https://doi.org/10.1016/j.matdes.2017.04.049
5. Miao S, Castro N, Nowicki M et al (2017) 4D printing of polymeric materials for tissue and organ regeneration. Mater Today 20(10):577–591. https://doi.org/10.1016/j.mattod.2017.06.005
6. Cui C, Kim D, Pack MY et al (2020) 4-D printing of self-folding and unit-encapsulating 3-D microstructures as scaffolds for tissue-engineering applications. Biofabrication 12:045018. https://doi.org/10.1088/1758-5090/aba502
7. Murphy SV, De Coppi P, Atala A (2020) Opportunities and challenges of translational 3D bioprinting. Nat Biomed Eng 4(4):370–380. https://doi.org/10.1038/s41551-019-0471-7
8. Janbaz S, Hedayati R, Zadpoor AA (2016) Programming the shape-shifting of flat soft matter: from self-rolling/self-twisting materials to self-folding origami. Mater Horiz 3(6):536–547. https://doi.org/10.1039/C6MH00195E
9. Jin Y, Gao Q, Xie C et al (2020) Fabrication of heterogeneous scaffolds using melt electrospinning writing: design and optimization. Mater Design 185:108274. https://doi.org/10.1016/j.matdes.2019.108274
10. Aghajani M, Wang M, Cox LM et al (2018) Influence of support-layer deformation on the intrinsic resistance of thin film composite membranes. J Membrane Sci 567:49–57. https://doi.org/10.1016/j.memsci.2018.09.031
11. van Manen T, Janbaz S, Zadpoor AA (2017) Programming 2D/3D shape-shifting with hobbyist 3D printers. Mater Horiz 4(6):1064–1069. https://doi.org/10.1039/C7MH00269F
12. Ge Q, Westbrook KK, Mather PT et al (2013) Thermomechanical behavior of a two-way shape memory composite actuator. Smart Mater Struct 22:055009. https://doi.org/10.1088/0964-1726/22/5/055009
13. Kirstie RR, Michael PD, Craig EB (2021) Future of additive manufacturing: overview of 4D and 3D printed smart and advanced materials and their applications. Chem Eng J 403:126162. https://doi.org/10.1016/j.cej.2020.126162

14. Wagner M, Chen T, Shea K (2017) Large shape transforming 4D auxetic structures. 3D Print Addit Manuf 4(3):133–141
15. Felton SM, Becker KP, Aukes DM et al (2015) Self-folding with shape memory composites at the millimeter scale. J Micromech Microeng 25:085004. https://doi.org/10.1088/0960-1317/25/8/085004
16. Zong L, Li MJ, Li CX (2017) Bioinspired coupling of inorganic layered nanomaterials with marine polysaccharides for efficient aqueous exfoliation and smart actuating hybrids. Adv Mater 29(10):1604691. https://doi.org/10.1002/adma.201604691
17. Deng H, Zhang C, Su JW et al (2018) Bioinspired multi-responsive soft actuators controlled by laser tailored graphene structures. J Mater Chem B 6:5415–5423. https://doi.org/10.1039/C8TB01285G
18. Janbaz S, Hedayati R, Zadpoor AA (2018) Programming the shape-shifting of flat soft matter. Mater Today 21(2):144–163. https://doi.org/10.1039/C6MH00195E
19. Hawkes E, An B, Benbernou NM et al (2010) Programmable matter by folding. PNAS 107(28):12441–12445. https://doi.org/10.1073/pnas.0914069107
20. Yuan C, Wang T, Dunn ML et al (2017) 3D printed bio-inspired origami with complicated folding patterns. Int J Jpn S Prec Eng 4(3):281–289. https://doi.org/10.1007/s40684-017-0034-x
21. Westbrook KK, Kao PH, Castro F et al (2011) A 3D finite deformation constitutive model for amorphous shape memory polymers: a multi-branch modeling approach for nonequilibrium relaxation processes. Mech Mater 43(12):853–869. https://doi.org/10.1016/j.mechmat.2011.09.004
22. Hu GF, Damanpack AR, Bodaghi M et al (2017) Increasing dimension of structures by 4D printing shape memory polymers via fused deposition modeling. Smart Mater Struct 26:125023. https://doi.org/10.1088/1361-665X/aa95ec
23. Zhang Q, Zhang K, Hu GK (2016) Smart three-dimensional lightweight structure triggered from a thin composite sheet via 3D printing technique. Sci Rep-UK 6:22431. https://doi.org/10.1038/srep22431
24. Wu H, Chen P, Yan C et al (2019) Four-dimensional printing of a novel acrylate-based shape memory polymer using digital light processing. Mater Des 171:107704. https://doi.org/10.1016/j.matdes.2019.107704
25. Manen T, Janbaz S, Ganjian M et al (2020) Kirigami-enabled self-folding origami Mater Today 32:59–67. https://doi.org/10.1016/j.mattod.2019.08.001
26. Damanpack AR, Bodaghi M, Liao WH (2020) Contact/impact modeling and analysis of 4D printed shape memory polymer beams. Smart Mater Struct 29:085016. https://doi.org/10.1088/1361-665X/ab8883a
27. Deng D, Yang Y, Chen Y et al (2017) Accurately controlled sequential self-folding structures by polystyrene film. Smart Mater Struct 26(8):085040. https://doi.org/10.1088/1361-665X/aa7a4e
28. Ge Q, Qi HJ, Dunn ML (2013) Active materials by four-dimension printing. Appl Phys Lett 103:131901. https://doi.org/10.1063/1.4819837
29. Goo B, Hong C, Park K (2020) 4D printing using anisotropic thermal deformation of 3D-printed thermoplastic parts. Mater Des 188:108485. https://doi.org/10.1016/j.matdes.2020.108485
30. Liu YP, Gall K, Dunn ML et al (2006) Thermomechanics of shape memory polymers: uniaxial experiments and constitutive modeling. Int J Plasticity 22(2):279–313. https://doi.org/10.1016/j.ijplas.2005.03.004
31. Lu HB, Wang XD, Yao YT et al (2018) A "frozen volume" transition model and working mechanism for the shape memory effect in amorphous polymers. Smart Mater Struct 27(6):065023. https://doi.org/10.1088/1361-665X/aab8af
32. Ge Q, Dunn CK, Qi HJ et al (2014) Active origami by 4D printing. Smart Mater Struct 23:094007. https://doi.org/10.1088/0964-1726/23/9/094007
33. Zhang Y, Zhang N, Hingorani H et al (2019) Fast-response, stiffness-tunable soft actuator by hybrid multimaterial 3D printing. Adv Funct Mater 29(15):1806698. https://doi.org/10.1002/adfm.201806698
34. Deng D, Chen Y (2015) Origami-based self-folding structure design and fabrication using projection based stereolithography. J Mech Des 137(2):021701. https://doi.org/10.1115/1.4029066
35. Bodaghi M, Damanpack AR, Liao WH (2016) Self-expanding/shrinking structures by 4D printing. Smart Mater Struct 25:105034. https://doi.org/10.1088/0964-1726/25/10/105034
36. Bodaghi M, Damanpack AR, Liao WH (2017) Adaptive metamaterials by functionally graded 4D printing. Mater Des 135:26–36. https://doi.org/10.1016/j.matdes.2017.08.069
37. Lu HB, Wang XD, Yu K (2017) A phenomenological formulation for shape/temperature memory effect in amorphous polymers with multi stress components. Smart Mater Struct 26(9):095011. https://doi.org/10.1088/1361-665X/aa77b3
38. Berthelin C, Kellner K, Mathieu M (2000) Storage metabolism in the Pacific oyster (Crassostrea gigas) in relation to summer mortalities and reproductive cycle (West Coast of France). Comp Biochem Phys B 125(3):359–369. https://doi.org/10.1016/S0305-0491(99)00187-X
39. Zeng S, Gao Y, Feng Y et al (2019) Programming the deformation of a temperature-driven bilayer structure in 4D printing. Smart Mater Struct 28:10503110
40. Ding Z, Weeger O, Qi HJ et al (2018) 4D rods: 3D structures via programmable 1D composite rods. Mater Des 137:256–265. https://doi.org/10.1016/j.matdes.2017.10.004
41. Luo WT, Zhang JF, Feng PF et al (2020) A concise peephole model based transfer learning method for small sample temporal feature-based data-driven quality analysis. Knowl-Based Syst 195:105665. https://doi.org/10.1016/j.knosys.2020.105665
42. Baker AB, Bates SRG, Llewellyn-Jones TM et al (2019) 4D printing with robust thermoplastic polyurethane hydrogel-elastomer trilayers. Mater Des 163:107544. https://doi.org/10.1016/j.matdes.2018.107544
43. Timoshenko S (1925) Analysis of bi-metal thermostats. J Optical Soc Am 11(3):233–255. https://doi.org/10.1364/JOSA.11.000233